ADVANCES IN ATMOSPHERIC SCIENCES, VOL. 23, NO. 5, 2006, 792–801

Implementation of the Semi-Lagrangian Advection Scheme on a Quasi-Uniform Overset Grid on a Sphere

LI Xingliang*[1,2] (李兴良), CHEN Dehui[2] (陈德辉), PENG Xindong[3] (彭新东),
XIAO Feng[2,4] (肖 锋), and CHEN Xiongshan[5] (陈雄山)

[1] *Nanjing University of Information Science and Technology, Nanjing* 210044

[2] *State Key Laboratory of Severe Weather, Chinese Academy of Meteorological Sciences, Beijing* 100081

[3] *Earth Simulator Center, Japan Agency for Marine-earth Science and Technology, Yokohama, Japan*

[4] *Tokyo Institute of Technology, Yokohama, Japan*

[5] *Institute of Atmospheric Physics, Chinese Academy of Sciences, Beijing* 100029

(Received 20 December 2005; revised 23 February 2006)

ABSTRACT

The semi-Lagrangian advection scheme is implemented on a new quasi-uniform overset (Yin-Yang) grid on the sphere. The Yin-Yang grid is a newly developed grid system in spherical geometry with two perpendicularly-oriented latitude-longitude grid components (called Yin and Yang respectively) that overlapp each other, and this effectively avoids the coordinate singularity and the grid convergence near the poles. In this overset grid, the way of transferring data between the Yin and Yang components is the key to maintaining the accuracy and robustness in numerical solutions. A numerical interpolation for boundary data exchange, which maintains the accuracy of the original advection scheme and is computationally efficient, is given in this paper. A standard test of the solid-body advection proposed by Williamson is carried out on the Yin-Yang grid. Numerical results show that the quasi-uniform Yin-Yang grid can get around the problems near the poles, and the numerical accuracy in the original semi-Lagrangian scheme is effectively maintained in the Yin-Yang grid.

Key words: Yin-Yang grid, semi-Lagrangian scheme, spherical geometry

doi: 10.1007/s00376-006-0792-9

1. Introduction

An advection transport plays one of the most important roles in atmospheric dynamics. As a matter of fact, the properties of an advection scheme are key for the proper representation of fluid dynamical phenomena in atmospheric numerical models. At the same time, most atmospheric numerical models are developed based on spherical geometry and adopt the finite difference scheme or spectral method to compute advection. The models suffer from the rigid limitation of the Courant-Friedrich-Lev (CFL) number and large computational errors due to the polar singularity in the latitude-longitude (LAT/LON) grid, which is especially serious when the grid resolution is refined. For instance, this is the case for the high resolution global mesoscale simulation with a 10-km grid (Ohfuchi et al., 2004). So far, two attempts, namely the application of the semi-Lagrangian advection scheme and the adoption of a uniform grid system, have been made to eliminate the pole singularity in the LAT/LON grid, and they have been found to be practical in improving the numerical accuracy and computational efficiency.

Since the publication of the pioneering work of Wiin-Nielsen (1959), the semi-Lagrangian scheme has received much attention for its superiority in computational stability and efficiency for large time steps. With this approach, Robert (1981, 1982) obtained stable integrations of both the divergent and non-divergent shallow water equations with a time step of up to 2 hours, using a semi-Lagrangian, semi-implicit grid-point model. Since then, Ritchie (1985, 1987), Rood (1987), McDonald (1984，1986), McDonald and Bates (1987，1989) have shown the numerical accuracy, computational stability and efficiency of the semi-Lagrangian scheme. Staniforth and Côté (1991)

*E-mail: lixliang@126.com

gave a detailed review of this method and its applications to numerical models for atmospheric dynamics. Compared with the Eulerian scheme, the time step of the semi-Lagrangian scheme can be free of the constraint of the CFL condition due to the computational stability. Robert (1981, 1982) showed that the time step could be four to six times as large as the maximum permitted for an equivalent Eulerian semi-implicit model. It has been also observed that semi-Lagrangian schemes are very accurate in numerical dispersion. Williamson and Rasch (1989) carried out a series of two-dimensional, shape-preserving semi-Lagrangian schemes with cubic and rational Hermite interpolations. We adopt the cubic Lagrange method to interpolate the physical values at the departure point since it gives a good trade-off between numerical accuracy and computational efficency.

The singularity and the convergence of meridians in the polar regions of the LAT/LON grid system still remain major obstacles to obtain more accurate and more efficient computations. The coordinate singularity, however, is not an actual physical singularity. As one of the circumventions, special measures of the departure points on the poles are developed, such as the way of McDonald and Bates (1989) to diagnose the polar wind using a minimization principle. The problem of the grid convergence is more serious. The convergence of meridians in the polar regions of the LAT/LON grid brings about real problems in computational stability and numerical accuracy. Making use of uniformly spaced grids is one of the solutions to this issue, for example, the icosahedral geodesic grid (Tomita et al., 2001) and the conformal-cubic grid (Rancic et al., 1996). These grids are generated in a manner more sophisticated than the LAT/LON grid.

Another approach is known as the "Yin-Yang" grid, which was suggested by Kageyama and Sato (2004) as a quasi-uniform overset grid without a singular point. A Yin-Yang grid is constructed by overlapping two perpendicularly oriented latitude-longitude grid components. Thus, existing numerical frameworks developed in the LAT/LON grid can be transplanted to the Yin-Yang grid in a more straightforward way. However, data exchange between the Yin and Yang zones on the boundaries is necessary in the Yin-Yang system, and this substantially affects the numerical solutions. Peng et al. (2006) developed a conservative constraint for the Yin-Yang grid by using the Eulerian time integration and the CIP-CSLR (Constrained Interpolation Profile-Conservative Semi-Lagrangian scheme with Rational function) advection algorithm (Xiao et al., 2002) to ensure the conservativeness across the Yin/Yang boundaries.

In this paper, a semi-Lagrangian advection scheme is developed in the Yin-Yang grid. The data exchange on the boundaries and the effect on the computational accuracy are investigated. The semi-Lagrangian advection scheme (Ritchie and Beaudoin, 1994) is adapted to the Yin-Yang grid and is implemented for a two-dimensional advection discretizing on the C-grid (Arakawa and Lamb, 1977). A standard test case of solid-body advection (Williamson et al., 1992) is also illustrated to show the accuracy of a numerical algorithm that uses the cubic Lagrange interpolation method.

This paper is organized as follows. A brief description of the Yin-Yang grid will be presented in the next section. Section 3 gives a detailed discussion of the semi-Lagrangian advection scheme. In section 4, a detailed description on the boundary data exchange will be given. The two-dimensional advection test is given in section 5 to evaluate the presented semi-Lagrangian scheme and the numerical method to transfer data across the Yin-Yang boundaries. Section 6 gives a standard test of the solid body advection proposed by Williamson et al. (1992). Finally, some remarks end the paper in section 7.

2. The Yin-Yang grid

The Yin-Yang grid (Kageyama and Sato, 2004) is an overset grid in spherical geometry, which consists of two notched latitude-longitude grids that are normal to each other (Fig. 1). The component (Yin- or Yang-) grid is selected to be the low latitude part of the LAT/LON grid. The composition of the two component grids, with one of the components being perpendicular to the other, covers the globe by overlapping. A component grid, say the Yang grid, is defined in spherical coordinates by

$$\begin{cases} \varphi : \varphi_{\min} = -\pi/4 \leqslant \varphi \leqslant \varphi_{\min} = \pi/4 \,, \\ \lambda : \lambda_{\min} = \pi/4 \leqslant \lambda \leqslant \lambda_{\min} = 7\pi/4 \,, \end{cases} \tag{2.1}$$

where φ is the latitude and λ the longitude.

The relationship between the Yin coordinate and the Yang coordinate is denoted in Cartesian coordinates by

$$(x_{\rm n}, y_{\rm n}, z_{\rm n}) = (-x_{\rm e}, z_{\rm e}, y_{\rm e}) \,, \tag{2.2}$$

where the subscript e denotes the Yin grid and n denotes the Yang grid.

From Eq. (2.2), we have the following relationships in spherical coordinates,

$$\begin{aligned} & r_n = r_e \,, \\ & \cos\varphi_n \cos\lambda_n = -\cos\varphi_e \cos\lambda_e \,, \\ & \cos\varphi_n \sin\lambda_n = \sin\varphi_e \,, \\ & \sin\varphi_n = \cos\varphi_e \sin\lambda_e \,, \end{aligned} \tag{2.3}$$

where and $(r_e, \varphi_e, \lambda_e)$ and $(r_n, \varphi_n, \lambda_n)$ are the coordinates of Yin and Yang, respectively.

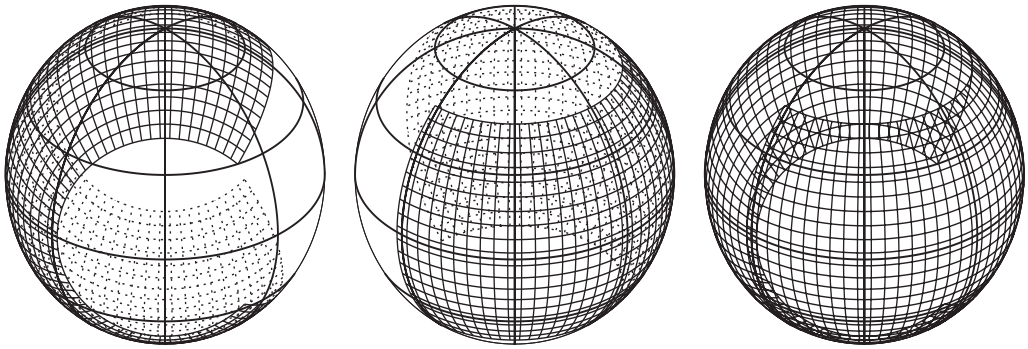

Fig. 1. Schematic diagram of the Yin-Yang grid. The Yin grid is shown on the left, the Yang grid in the middle and their composition on the right.

For spatial discretization, we have an expression of the Yin-Yang grid,

$$\begin{cases} \varphi_{\Gamma j} = \varphi_{\min} + j\Delta\varphi\,, \ \ (j = 0,\ N_\varphi - 1)\,, \\ \lambda_{\Gamma i} = \lambda_{\min} + i\Delta\lambda\,, \ \ (i = 0,\ N_\lambda - 1)\,, \end{cases} \tag{2.4}$$

and

$$\begin{cases} \Delta\varphi = (\varphi_{\max} - \varphi_{\min})/(N_\varphi - 1)\,, \\ \Delta\lambda = (\lambda_{\max} - \lambda_{\min})/(N_\lambda - 1)\,, \end{cases} \tag{2.5}$$

where N_φ and N_λ denote the mesh point numbers of the longitude and latitude, respectively. Γ =n is the Yang grid, and Γ =e is the Yin grid.

An important feature of the Yin-Yang grid as an overset grid is that the two component grids are identical and orthogonal, which may be beneficially used with many mature numerical techniques developed for a structured grid. The grid spacing of the Yin-Yang grid is quasi-uniform, and the ratio of the minimum/maximum grid spacings is approximately 0.707. Furthermore, there are no longer singularities in the Yin-Yang grid. Another advantage of the Yin-Yang grid is that the component grid is nothing but a part of the ordinary LAT/LON grid. We can make use of the existing numerical codes including parallel codes and tools developed for the LAT/LON grid. All of these properties make the numerical computation in the Yin-Yang grid more efficient and accurate in comparison with that on the LAT/LON grid.

3. Semi-Lagrangian advection scheme

3.1 *Semi-Lagrangian method*

The Lagrange-type transport equation for the scalar $F(\boldsymbol{x}, t)$ can be written as

$$\frac{DF}{Dt} = 0\,, \tag{3.1}$$

where D/Dt is the substantial derivative, $\boldsymbol{x}$ the position vector and t the time.

The solution of (3.1) is generally expressed as

$$F_{\tau+1}(\boldsymbol{x}, t + \Delta t) = F_{d,\tau}(\boldsymbol{x} - \alpha, t) \tag{3.2}$$

where Δt is the time step, and the subscript "d" denotes the departure point of the foot trajectory. The subscripts "τ" and "$\tau + 1$" denote the current and the next time steps respectively. The value of $\alpha = \boldsymbol{x}(t + \Delta t) - \boldsymbol{x}(t)$ can be obtained from

$$\frac{D\boldsymbol{x}}{Dt} = \boldsymbol{u}(\boldsymbol{x}, t) \tag{3.3}$$

or in the integration form

$$x_{\rm a} - x_{\rm d} = \int_{\Delta t}^{(\tau+1)\Delta t} u dt = \overline{u}\Delta t \tag{3.4}$$

where $\boldsymbol{u}(\boldsymbol{x}, t)$ denotes the wind field and the subscript "a" denotes the arrival point of the trajectory.

3.2 *The algorithms of the departure-point calculation in spherical geometry*

3.2.1 *Ritchie and Beaudoin's algorithm*

The spherical departure-point calculation in the HPE (hydrostatic primitive equation) shallow-atmosphere case was proposed by Ritchie (1987) and then extended to the non-hydrostatic primitive equation by Ritchie and Beaudoin (1994), where efforts were made to reduce the computational cost of the trigonometric functions. We summarize the numerical procedure of Ritchie and Beaudoin's algorithm as follows:

(1) Solve (u_0, v_0) with

$$\lambda_0 = \lambda_{\rm a} - \frac{u_0\Delta t}{2r_{\rm a}\cos\varphi_2}\left[1 + \frac{\Delta t^2}{24r_{\rm a}^2}(u_0^2\tan^2\varphi_{\rm a} - v_0^2)\right]\,, \tag{3.5}$$

and

$$\varphi_0 = \varphi_{\rm a} - \frac{v_0\Delta t}{2r_{\rm a}} + \left(\frac{u_0\Delta t}{2r_{\rm a}}\right)^2\frac{\tan\varphi_{\rm a}}{2}\,, \tag{3.6}$$

iteratively for $(\lambda_0, \varphi_0), (u_0, v_0)$;

(2) Calculate $\lambda_{\rm d}$ and $\varphi_{\rm d}$ with

$$\lambda_{\rm d} = \lambda_{\rm a} - \frac{u_0\Delta t}{a\cos\varphi_{\rm a}}\left[1 - \left(\frac{v_0\Delta t}{2r_{\rm a}}\right)\tan\varphi_{\rm a}\right]\,, \tag{3.7}$$

and

$$\varphi_{\rm d} = \varphi_{\rm a} - \frac{v_0\Delta t}{r_{\rm a}} + \left(\sec^2\varphi_{\rm a} - \frac{2}{3}\right)\left(\frac{u_0\Delta t}{2r_{\rm a}}\right)^2 \frac{v_0\Delta t}{2r_{\rm a}}\,, \tag{3.8}$$

where $u_0, v_0, \lambda_0, \varphi_0, \lambda_{\rm a}, \varphi_{\rm a}, \lambda_{\rm d}, \varphi_{\rm d}$ denote the mid-point velocity components, the mid-point longitude and latitude, the longitude and latitude of the departure and arrival point C, respectively, and $r_{\rm a}$ is the earth radius.

We use the simplified version of (3.5)–(3.8) to define all arrival points. Only the linear terms of Δt are retained in this paper because the curvature terms for the chosen latitude and longitude are quite small.

3.2.2 *McDonald and Bates' algorithm*

From equations (3.5)–(3.8), we observe that the procedure of the Ritchie and Beaudoin (1994) algorithm breaks down near the poles. Terms with $\tan\varphi_{\rm a}$ and $\sec\varphi_{\rm a}$ reach infinity at the poles. For efficient computation, we use the rotated grid method of McDonald and Bates (1989) to locate the departure points for latitudes over 80 degrees. The essence of the method is to use local orthogonal great circles at each arrival point to define a new coordinate system in which the departure point calculation is performed. Let primes denote quantities evaluated in the rotated latitude/longitude system having its origin at $\lambda' = 0, \varphi' = 0$. The McDonald and Bates (1989) algorithm can be described as follows:

(1) The coordinates of the departure point in the rotated system can be obtained from

$$\lambda'_{\rm d} = -\frac{u'_0\Delta t}{r_{\rm a}\cos\varphi'_0}\,, \tag{3.9}$$

$$\varphi'_{\rm d} = -\frac{v'_0\Delta t}{r_{\rm a}}\,, \tag{3.10}$$

where a is the earth radius.

(2) The latitude φ'_0 and the velocity components u'_0, v'_0 are evaluated at the midpoint of the great circle arc between the departure point and the arrival point.

$$\lambda'_0 = \lambda'_{\rm d}/2\,, \tag{3.11}$$

$$\varphi'_0 = \varphi'_{\rm d}/2\,, \tag{3.12}$$

(3) It is easy to use (3.11) and (3.12) with (3.9) and (3.10) to determine $\lambda'_{\rm d}, \varphi'_{\rm d}$ iteratively in the rotated coordinates. The departure point in the original coordinates is found by transformations expressed in (3.13) and (3.14):

$$\lambda_{\rm d} = \lambda_{\rm a} + \tan^{-1}\left(\frac{\cos\varphi'_{\rm d}\sin\lambda'_{\rm d}}{\cos\varphi'_{\rm d}\cos\lambda'_{\rm d}\cos\varphi_{\rm a} - \sin\varphi'_{\rm d}\sin\varphi_{\rm a}}\right)\,, \tag{3.13}$$

$$\varphi_{\rm d} = \arcsin(\cos\varphi'_{\rm d}\cos\lambda'_{\rm d}\sin\varphi_{\rm a} + \sin\varphi'_{\rm d}\cos\varphi_{\rm a})\,. \tag{3.14}$$

Because the data we need to interpolate the midpoint λ'_0, φ'_0 are in the original coordinates, it is necessary to transform both coordinates and velocity components between the grids at each iteration as follows,

$$u'_0 = Gu_0 - Sv_0\,, \tag{3.15}$$

$$v'_0 = Su_0 + Gv_0\,, \tag{3.16}$$

$$G = [\cos\varphi\cos\varphi_{\rm a} + \sin\varphi\cos(\lambda - \lambda_{\rm a})\sin\varphi_{\rm a}]/\cos\varphi'\,, \tag{3.17}$$

$$S = [\sin\varphi_{\rm a}\sin(\lambda - \lambda_{\rm a})]/\cos\varphi'\,, \tag{3.18}$$

where φ and λ is the midpoint latitude and longitude in the original system, φ' is the midpoint latitude in the rotated system, and $\varphi_{\rm a}$ is the departure-point latitude. Equations (3.11) and (3.12) are sufficiently accurate because the rotated system causes all computations to be carried out in the vicinity of the equator.

4. Cubic Lagrange interpolation and boundary data exchange in the Yin-Yang grid

4.1 *Cubic Lagrange interpolation*

We need to interpolate the departure-point values after finding the departure points. The widely used interpolation methods are cubic spline interploation and cubic Lagrange interpolation. We adopt the cubic Lagrange method to interpolate the departure-point values since it provides adequate numerical accuracy for most applications and is computationally efficient.

Let $x_0, x_1, \ldots, x_n$ be $n+1$ distinct points in one dimension, where a real function $f(x)$ is defined; we consider a one-dimensional polynomial interpolation function $q(x)$ of nth-order. With the collocation conditions

$$f(x_k) = q(x_k), \text{for each } k = 0, 1, \ldots, n,$$

one may uniquely find the interpolation polynomial as

$$q_n(x) = a_0 + a_1 x + \cdots + a_n x^n\,. \tag{4.1}$$

Using the Lagrange interpolation, we define the base function $l_i(x)$ as

$$l_i(x) = \prod_{\substack{j=0\\ j\neq i}}^{n} \frac{x - x_j}{x_i - x_j}\,, \quad (i = 0, 1, \cdots, n)\,. \tag{4.2}$$

The corresponding bases for one-dimensional cubic La-

grange interpolation are

$$l_0(x) = \frac{(x-x_1)(x-x_2)(x-x_3)}{(x_0-x_1)(x_0-x_2)(x_0-x_3)} , \tag{4.3}$$

$$l_1(x) = \frac{(x-x_0)(x-x_2)(x-x_3)}{(x_1-x_0)(x_1-x_2)(x_1-x_3)} , \tag{4.4}$$

$$l_2(x) = \frac{(x-x_1)(x-x_0)(x-x_3)}{(x_2-x_1)(x_2-x_0)(x_2-x_3)} , \tag{4.5}$$

$$l_3(x) = \frac{(x-x_1)(x-x_2)(x-x_0)}{(x_3-x_1)(x_3-x_2)(x_3-x_0)} , \tag{4.6}$$

Then, the one-dimensional cubic Lagrange interpolation polynomial is

$$q_3(x) = l_0 y_0 + l_1 y_1 + l_2 y_2 + l_3 y_3 , \tag{4.7}$$

where y_i $(i = 0, 1, 2, 3)$ are the values of $f(x)$ at the corresponding points.

For a two-dimensional bi-cubic Lagrange interpolation, as shown in Fig. 2a, 16 points are required for the interpolation. Suppose $q(x, y)$ is the interpolated point; we first obtain the values at the cross points a, b, c, d along the x direction by using one-dimensional cubic Lagrange interpolation, then we interpolate the $q(x, y)$ values along the y direction by using the computed values at a, b, c, d. The detailed formulae are

$$\begin{aligned} q_{\rm a}(x_{\rm a}, y_{\rm a}) =& l_{\rm a0} q(i-1, j-1) + l_{a1} q(i, j-1) + \\ & l_{\rm a2} q(i+1, j-1) + l_{\rm a3} q(i+2, j-1) , \end{aligned} \tag{4.8}$$

$$\begin{aligned} q_b(x_b, y_b) =& l_{b0} q(i-1, j) + l_{b1} q(i, j) + \\ & l_{b2} q(i+1, j) + l_{b3} q(i+2, j) , \end{aligned} \tag{4.9}$$

$$\begin{aligned} q_{\rm c}(x_{\rm c}, y_{\rm c}) =& l_{\rm c0} q(i-1, j+1) + l_{\rm c1} q(i, j+1) + \\ & l_{c2} q(i+1, j+1) + l_{c3} q(i+2, j+1) , \end{aligned} \tag{4.10}$$

$$\begin{aligned} q_{\rm d}(x_{\rm d}, y_{\rm d}) =& l_{d0} q(i-1, j+2) + l_{d1} q(i, j+2) + \\ & l_{d2} q(i+1, j+2) + l_{d3} q(i+2, j+2) , \end{aligned} \tag{4.11}$$

$$\begin{aligned} q(x, y) =& l_{\rm q0} q(x_{\rm a}, y_{\rm a}) + l_{\rm q1} q(x_{\rm b}, y_{\rm b}) + \\ & l_{\rm q2} q(x_{\rm c}, y_{\rm c}) + l_{\rm q3} q(x_{\rm d}, y_{\rm d}) , \end{aligned} \tag{4.12}$$

where $l_{{\rm a}k}, l_{{\rm b}k}, l_{{\rm c}k}, l_{{\rm d}k}, l_{{\rm q}k}$ $(k = 0, 1, 2, 3)$ are the base functions corresponding to the a, b, c d points.

4.2 *Boundary data exchange of the Yin-Yang-grid*

As an overset grid system, the Yin-Yang grid needs to exchange the boundary data on the overlapping borders. For the convenience of discussion, we divide the points of one component grid into the interior points and the boundary points on the overlapping borders. For a semi-Lagrangian advection scheme, the departure points on the boundary grid points may be traced into another component grid. The values of the departure points can be interpolated with the values at the points of another component grid. The departure points of interior points on each component grid generally are located within the same component grid. We can adopt the conventional method similar to the LAT/LON grid to compute the value of the departure-point.

In section 2, the scope of the Yin-Yang grid is defined to be from 45°S $(-\pi/4)$ to 45°N $(\pi/4)$ in the latitudinal direction and from 45°E $(\pi/4)$ to 45°W $(7\pi/4)$ in the longitudinal direction, which minimizes the overlapping region at the Yin-Yang borders. However, in order to carry out the semi-Lagrangian computation for each component grid, one needs to extend the scope of each component to cover the region where the departure points of the boundary point from the same component grid may reach. As shown in Fig. 2b, the dashed lines indicate the extended boundary region of the Yin grid. The departure point of the boundary point A in the Yin grid, for example, should be covered by the extended scope. So, the value at the departure point of A can be found from an interpolation constructed in the same way as other interior points of the Yin grid. The values in the extended region for each component have to be interpolated from the values at the interior points of another component. We describe the detailed computational procedure that transfers the data from the Yang grid to the Yin grid as follows.

(1) Find the positions of all the boundary points of the Yin grid in the Yang grid.

(2) According to the positions of boundary points in the Yin grid with respect to the Yang grid, shown as dashed lines in Fig. 2b, decide the extended overlapping region.

(3) For each grid point P (the dark square in Fig. 2b, for example) in the extended Yin grid, the value is interpolated from the surrounding points of another component (the Yang) grid by using the cubic Lagrange method.

(4) For each boundary point A of the Yin grid, its departure point B is located in the extended region of the same Yin grid. We can interpolate the value at point B in the Yin grid through the conventional method similar to the LAT/LON grid.

The above procedures are carried out every time step so as to keep a minimal overlapping situation.

4.3 *Calculation of the mid-point wind for a boundary departure point*

Following the above procedure, interpolations are applied to each component grid to set the boundary values. When one is dealing with a vector field, special

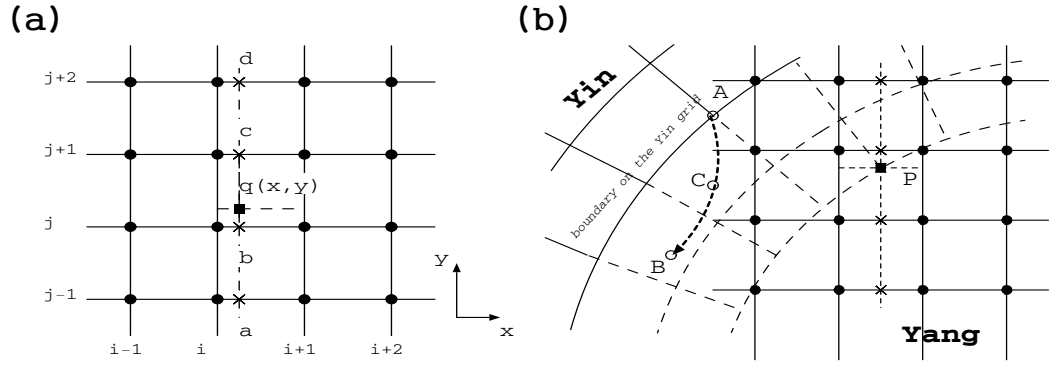

Fig. 2. Schematic diagram of (a) the two-dimensional cubic Lagrange interpolation and (b) the boundary interpolation diagram of the Yin-Yang grid.

care is needed for vector components because a vector has a different representation in the Yin or Yang coordinates. The calculation of the departure point involves the vector transformation between the Yin and Yang grids while one uses the semi-Lagrangian scheme, such as Ritchie and Beaudoin (1994) or McDonald and Bates (1989).

As shown in Fig. 2b, we compute the departure-point B based on the arrival grid point A and the velocity of the midpoint C at the half-time level in the spherical coordinates, using the algorithm of Ritchie and Beaudoin (1994). The detailed procedure is listed as follows.

(1) Compute the position of the middle point C at the half-time level in the spherical coordinates using the algorithm of Ritchie and Beaudoin (1994).

(2) If point C is located in the Yang grid, interpolate the velocity component value in the Yang grid.

(3) Transform the velocity at point C from the Yang grid to the Yin grid.

(4) Compute the departure point with (3.7) and (3.8) or (3.13) and (3.14).

With these steps, we have exchanged the boundary data between the Yin and Yang grids. The corresponding numerical tests are found in section 6.

5. Order-preserving test of the Yin-Yang grid

Shown above, the data transfer across the Yin/Yang boundaries is involved in the Yin-Yang grid. The interpolation procedure used in the data exchange may substantially affect the numerical accuracy. Thus, in this section, we evaluate the presented method with idealized advection experiments.

5.1 *Setup of the test*

We consider the pure advection equation in two dimensions:

$$\frac{dq}{dt} = 0 \,, \tag{5.1}$$

with the initial condition defined by

$$q(\varphi, \lambda) = q_0 \cos^2 \varphi \sin(k\lambda) \,, \tag{5.2}$$

where q_0 is a constant and k is the wave number.

In the latitude-longitude system, the wind is defined as

$$u = u_0(\cos\varphi\cos\alpha + \sin\varphi\cos\lambda\sin\alpha) \,, \tag{5.3}$$

$$v = -u_0 \sin\lambda \sin\varphi \,, \tag{5.4}$$

where the factor α is the angle between the direction of rotation and the polar axis of the spherical coordinate system. The test presented in this paper was run with $\alpha = 0$ and $u_0 = 2\pi r_{\rm a}/(12\ {\rm d})$.

The numerical advection with different resolutions is conducted to examine the numerical errors and the convergence rate in terms of grid refinement. Resolutions of $0.625^\circ \times 0.625^\circ, 1.25^\circ \times 1.25^\circ$, and $2.5^\circ \times 2.5^\circ$ and the corresponding time steps of 2400 s, 4800 s, and 9600 s are used. Numerical results after one, two and four revolutions are given to show the errors in phase and amplitude. For comparison, we carried out the numerical integrations on both the Yin-Yang grid and the conventional LAT/LON grid separately. The Ritchie and Beaudoin (1994) algorithm is used for advection in the Yin-Yang grid and for the low latitude region (between 80°S and 80°N) in the LAT/LON grid, while the McDonald and Bates scheme (1989) is adopted for the high latitude region in the LAT/LON grid to locate the departure points. The cubic Lagrange interpolation and Arakawa-C spatial discretization are used on the two grid systems.

5.2 *Results of the order-preserving test*

Following Takacs (1984) and Bermejo and Staniforth (1992), a measure of the total error based on an ℓ_1 norm is given as

$$E_{\ell_1} = \frac{1}{N} \sum_N |q(\varphi, \lambda) - q_{\rm T}(\varphi, \lambda)| \,, \tag{5.5}$$

and the convergence rate ε due to the grid refinement

Table 1. E_{ℓ_1} errors on the Yin-Yang grid and LAT/LON grid.

Resolution	$0.625^\circ \times 0.625^\circ$	$1.25^\circ \times 1.25^\circ$	$2.5^\circ \times 2.5^\circ$
Yin-Yang grid	0.9761×10^{-4}	0.8350×10^{-3}	0.6921×10^{-2}
LAT/LON grid	0.2644×10^{-4}	0.2168×10^{-3}	0.1778×10^{-2}

Table 2. Convergence rate ε on the Yin-Yang grid and LAT/LON grid.

Resolution	ε (2.5/0.625)	ε (2.5/1.25)
Yin-Yang grid	3.07390	3.05111
LAT/LON grid	3.03585	3.03579

is defined as

$$\varepsilon(\Delta x_2/\Delta x_1)=\ln[E_{\ell_1}(\Delta x_2)/E_{\ell_1}(\Delta x_1)]/\ln(\Delta x_2/\Delta x_1)\,, \tag{5.6}$$

where N is the total number of grid points and $q_{\rm T}$ is the true value.

Shown in Table 2, a 3rd-order accuracy is achieved on both the Yin-Yang grid and LAT/LON grid with the cubic Lagrange interpolation method. It is observed that the data transfer over the Yin-Yang boundaries does not degrade the convergence rate of the semi-Lagrangian scheme. It should also be noted that the numerical errors on the Yin-Yang grid are larger than those on the LAT/LON grid with the same resolution as shown in Table 1. Although this is a case in favor of the LAT/LON grid where the "solid body" is transported along the equator and the numerical error due to the meridional convergence is minimized, it reveals that the boundary interpolation involves extra numerical errors and is worthy of further investigation for all applications in the Yin-Yang grid.

6. Two-dimensional advection of a solid body

A two-dimensional advection test of a solid body with divergence-free current has been suggested by Williamson et al. (1992). It is also tested here on both the Yin-Yang grid and the LAT/LON grid.

6.1 *Design of the two-dimensional solid-body advection*

Similar to section 5, we consider the advection equation (5.1) with the wind field the same as (5.3) and (5.4). The solid body is defined as

$$q(\lambda,\varphi)=\begin{cases} 0.5[1+\cos(\pi r/R)]\,, & \text{if} \quad r<R=r_{\rm a}/3 \\ 0, & \text{if} \quad r\geqslant R=r_{\rm a}/3\,, \end{cases} \tag{6.1}$$

where $r = r_{\rm a}\cos^{-1}[\sin\varphi_0\sin\varphi+\cos\varphi_0\cos\varphi\cos(\lambda-\lambda_0)]$, $r_{\rm a}=6.37122\times10^6$ is the radius of the Earth, and (λ_0,φ_0) is the center of the solid body here, initially taken as $\lambda_0=\pi/2$ and $\varphi_0=0$.

Equatorial and polar advections with different resolutions are tested here for comparison between the two grids. The resolutions are selected to be $0.625^\circ\times0.625^\circ$, $1.25^\circ\times1.25^\circ$, and $2.5^\circ\times2.5^\circ$. The corresponding time steps are 2400 s, 4800 s, and 9600 s. Only one revolution is kept in all the tests. The semi-Lagrangian algorithm, polar treatment, interpolation method and spatial discretization are the same as in section 5.

6.2 *Results of the solid-body advection test*

Similar to Williamson et al. (1992), we define

$$\begin{aligned} I_{\text{Yin-Yang}}(q) =& \frac{1}{4\pi}\int_{\frac{\pi}{4}}^{\frac{7\pi}{4}}\int_{-\frac{\pi}{4}}^{\frac{\pi}{4}} q_{\rm Yang}(\lambda,\varphi)\cos\varphi d\varphi d\lambda + \\ & \frac{1}{4\pi}\int_{\frac{\pi}{4}}^{\frac{7\pi}{4}}\int_{-\frac{\pi}{4}}^{\frac{\pi}{4}} q_{\rm Yin}(\lambda,\varphi)\cos\varphi d\varphi d\lambda\,, \end{aligned} \tag{6.2}$$

where $q_{\rm Yin}$ and $q_{\rm Yang}$ are the densities of the transported material in the Yin and Yang grids, respectively. $I_{\text{Yin-Yang}}(q)$ denotes the total global mass integration. Numerical errors in the LON/LAT grid are evaluated by using two kinds of norms the same as in Williamson et al. (1992):

$$\ell_2(q)=\frac{\{I_{\text{Yin-Yang}}[(q(\lambda,\varphi)-q_{\rm T}(\lambda,\varphi))^2]\}^{\frac{1}{2}}}{\{I_{\text{Yin-Yang}}[q_{\rm T}(\lambda,\varphi)^2]\}^{\frac{1}{2}}}\,, \tag{6.3}$$

$$\ell_\infty(q)=\frac{\max[|q_{\rm Yang}(\lambda,\varphi)-q_{\text{Yang, T}}(\lambda,\varphi)|,|q_{\rm Yin}(\lambda,\varphi)-q_{\text{Yin, T}}(\lambda,\varphi)|]}{\max[|q_{\text{Yang, T}}(\lambda,\varphi)|,|q_{\text{Yin, T}}(\lambda,\varphi)|]}\,, \tag{6.4}$$

where $q_{\rm Yin}$ and $q_{\text{Yang, T}}$ are the initial mass values of the Yin grid and Yang grid, respectively.

In Fig. 3, we can observe that the ℓ_2 and ℓ_∞ errors of the two grid systems increase with integration time. In the Yin-Yang grid, the ℓ_2 and ℓ_∞ errors experience four pulse-like jumps when the solid body passes across the overlapping border, which is due to the numerical errors associated with the data transfer over the Yin-Yang boundaries. We find that the ℓ_2 and ℓ_∞ errors grow smoothly in the LAT/LON grid in the pole-ward advection, and decrease at day 3 and day 9, when the McDonald and Bates (1989) transformation is employ-

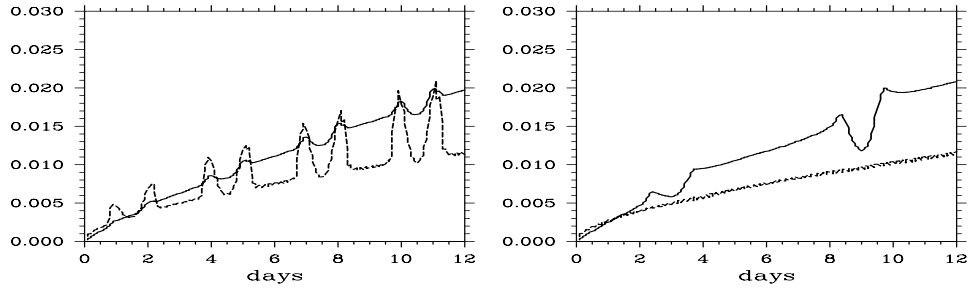

Fig. 3. Time series of the ℓ_2 (solid) and ℓ_∞ (dashed) errors in the poleward advection after one revolution around the globe with a $1.25^\circ \times 1.25^\circ$ resolution by the Yin-Yang grid (left) and the LAT/LON grid (right).

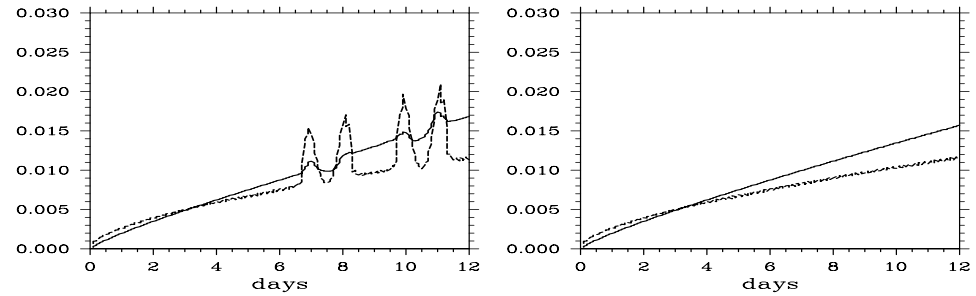

Fig. 4. Same as Fig. 3, but for equatorial advection.

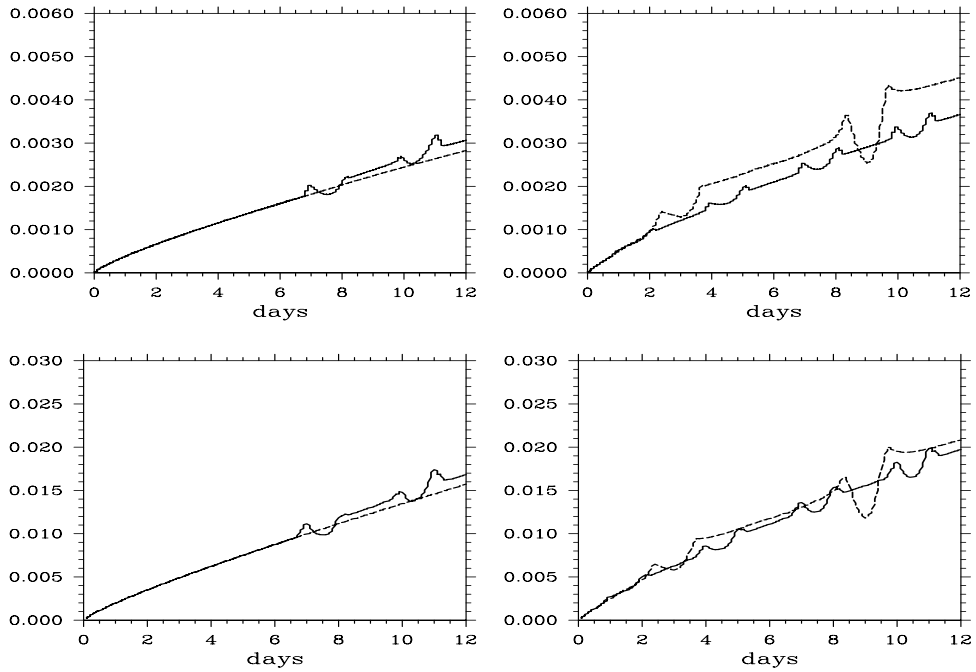

Fig. 5. Comparison of ℓ_2 errors on the Yin-Yang grid (solid) and LAT/LON grid (dashed) in different resolutions and transportation directions. Left panels show equatorial transport and the right ones are the poleward case. Top panels correspond to $0.625^\circ \times 0.625^\circ$ resolution and the bottom correspond to $1.25^\circ \times 1.25^\circ$ resolution.

ed. The computational time in the Yin-Yang grid, on the other hand, increases due to the additional interpolation and data transfer required. Similar results are observed in the case of equatorial advection (Fig. 4).

In Fig. 5, the ℓ_2 norms in different resolutions and different transport angles are given for the 12-day period on both the Yin-Yang and LAT/LON grids. No distinct difference is found between the two grid systems except for some local, small fluctuations in the errors. We noticed that the error norms decrease rapidly as the resolution increases. When the resolution is increased from $1.25^\circ \times 1.25^\circ$ to $0.625^\circ \times 0.625^\circ$, the ℓ_2 norm errors decreased to one-sixth of their original values. Under the cubic boundary interpolation, the errors in both grid systems are at the same level. In the case of equatorial transport, smaller error is observed in the LAT/LON grid. In the poleward transport, however, the ℓ_2 norm errors show that the Yin-Yang grid is more accurate than the LAT/LON grid even if the McDonald and Bates (1989) method is used in the polar region. Without the large-circle transformation (McDonald and Bates, 1989), the effects of the meridional convergence error and the polar singularity are more serious in the LAT/LON system. The experiment indicates that the Yin-Yang grid is more favorable than the LAT/LON grid in the case of high-resolution simulations, which can be verified from the illustrations in Fig. 5. On the other hand, the numerical solution is obviously sensitive to the boundary interpolation scheme. A higher order scheme is worth exploring to get more accurate results.

The results of the "solid body" during the poleward transport on the Yin-Yang grid are given in

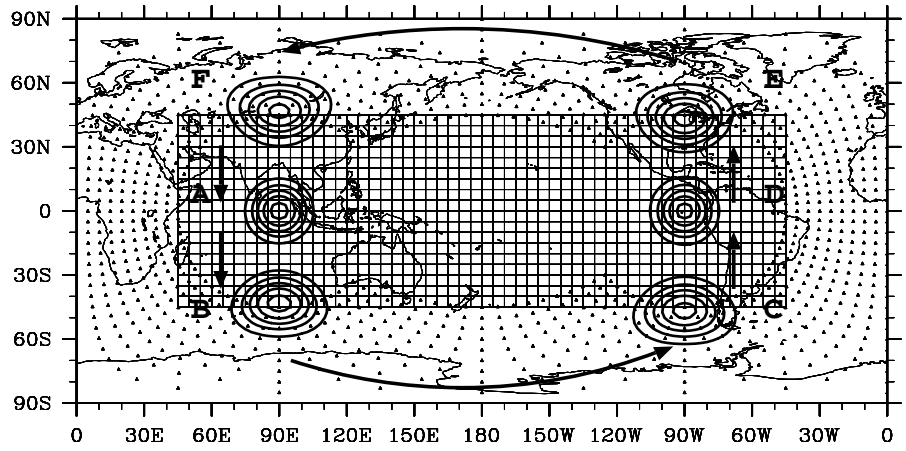

Fig. 6. Contour plots of the "solid body" during the advection with a resolution of $2.5^\circ \times 2.5^\circ$. The initial concentration passes across the overlapping border four times in the Yin-Yang system. The contours are plotted from 0.1 to 0.9 with an interval of 0.2. The mesh nodes indicate the grid point in the Yang grid, and the triangles mark the grid points in the Yin grid.

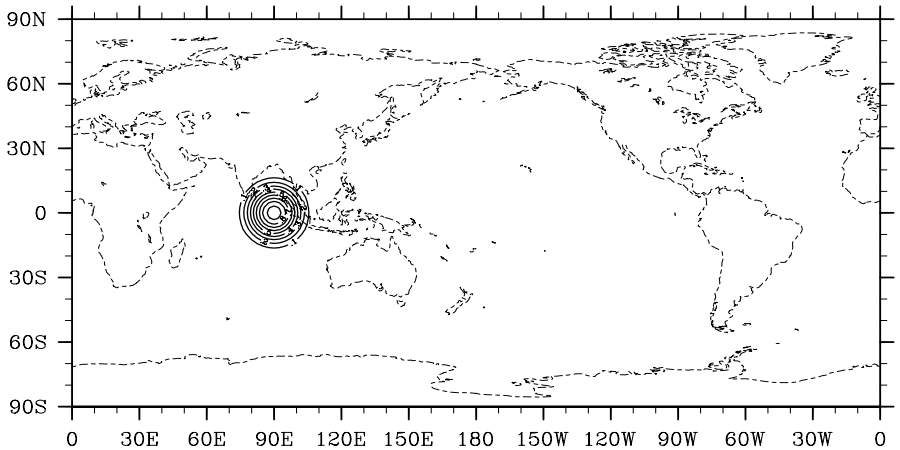

Fig. 7. The contour plots of the "solid body" after one revolution on the Yin-Yang grid with a resolution of $2.5^\circ \times 2.5^\circ$. The contours are plotted from 0.1 to 0.9 at an interval of 0.1.

Fig. 6, where B, C, D, E and F are numerical solutions at different instances and A is the initial (exact) distribution. The "solid body", starting from A, travels across the overlapping borders at B, C, D, E and F, and finally arrives back to its initial position after 12 days. From Fig. 7, we observe that the "solid body" adequately keeps its initial shape even after one poleward revolution. The singularity in the conventional LAT/LON grid is completely eliminated and the numerical advection is accurately computed.

7. Conclusion and remarks

The semi-Lagrangian advection scheme is developed for a new quasi-uniform and singularity-free Yin-Yang grid. A method for the boundary data exchange in the Yin-Yang grid is given and tested by idealized experiments in this paper. We use the cubic Lagrange interpolations for both the semi-Lagrangian scheme and the boundary data transfer computation. We show, with numerical experiments, that the resulting advection scheme on the Yin-Yang grid has 3rd-order accuracy. Another test with the "solid body" advection shows that the Yin-Yang grid is superior to the ordinary LAT/LON grid in the case of poleward advection. The Yin-Yang grid has a quasi-uniform grid spacing and does not include any singular region—like the polar zone in the LAT/LON grid—thus it can be one of the promising candidate grid systems for high resolution GCM simulations. Although the data exchange procedure is presented only for the pure advection in this paper, it also applies to other dynamical processes in the GCMs, and this will be reported in other papers.

Acknowledgments. We thank Xue Jishan, Shen Xueshun, Yang Xuesheng, Zhang Hongliang and Hu Jianglin for their kind help and discussions. This paper is sponsored by the National Natural Science Foundation of China (No. 40575050) and the National Key Program for Developing Basic Reseach ("973") (No. 2004CB418306).

REFERENCES

Arakawa, A., and V. R. Lamb, 1977: Computational design of the basic dynamical process of the UCLA general circulation model. *Methods in Computational Physics*., Vol. 17, J. Chang, Ed., Academic Press, San Francisco, USA, 173–265.

Bermejo, R., and A. Staniforth, 1992: The conversion of semi-Lagrangian advection schemes to quasi-monotone schemes. *Mon. Wea. Rev.*, **120**, 2622–2632.

Kageyama, A., and T. Sato, 2004: The "Yin-Yang grid": An overset grid in spherical geometry. *Geochem. Geophys. Geosyst.*, **5**, Q09005, dio:10.1029/2004GC000734.

McDonald, A., 1984: Accuracy of multiply-upstream, semi-Lagrangian advection schemes. *Mon. Wea. Rev.*, **112**, 1267–1275.

McDonald, A., 1987: Accuracy of multiply-upstream, semi-Lagrangian advection schemes, II. *Mon. Wea. Rev.*, **115**, 1446–1450.

McDonald, A., and J. R. Bates, 1987: Improving the estimate of the departure point position in a two-time-level semi-Lagrangian and semi-implicit model. *Mon. Wea. Rev.*, **115**, 737–739.

McDonald, A., and J. R. Bates, 1989: Semi-Lagrangian integration of a gridpoint shallow water model on the sphere. *Mon. Wea. Rev.*, **117**, 130–137.

Ohfuchi, W., and Coauthor, 2004: 10-km mesh meso-scale resolving simulations of the global atmosphere on the Earth Simulator—Preliminary outcomes of AFES (AGCM for the Earth Simulator). *J. Earth Simulator*, **1**, 5–31.

Peng, X., F. Xiao, and K. Takahashi, 2006: Conservative constraint for a quasi-uniform overset grid on sphere. *Quart. J. Roy. Meteor. Soc.*, **132**, 979–996.

Rancic, M., J. Purser, and F. Mesinger, 1996: A global shallow-water model using an expanded spherical cube: Gnomonic versus conformal coordinates. *Quart. J. Roy. Meteor. Soc.*, **122**, 959–982.

Ritchie, H., 1985: Application of a semi-Lagrangian integration scheme to the moisture equation in a regional forecast model. *Mon. Wea. Rev.*, **113**, 424–435.

Ritchie, H., 1987: Semi-Lagrangian advection on a Gaussian grid. *Mon. Wea. Rev.*, **115**, 608–619.

Ritchie, H., and C. Beaudoin, 1994: Approximations and sensitivity experiments with a baroclinic semi-Lagrangian spectral model. *Mon. Wea. Rev.*, **122**, 2391–2399.

Robert, A., 1981: A stable numerical integration scheme for the primitive meteorological equation. *Atmos. Ocean*, **19**, 35–46.

Robert, A., 1982: Semi-Lagrangian and semi-implicit numerical integration scheme for the primitive meteorological equation. *Quart. J. Roy. Meteor. Soc.*, **60**, 319–324.

Rood, R., 1987: Numerical advection algorithms and their role in atmospheric transport and chemistry models. *Rev. Geophys.*, **25**, 71–100.

Staniforth, A., and J. Côté, 1991: Semi-Lagrangian integration schemes for atmospheric models—A review. *Mon. Wea. Rev.*, **119**, 2206–2223.

Takacs, L. L., 1985: A two-step scheme for the advection equation with minimized dissipation and dispersion errors, *Mon. Wea. Rev.*, **113**, 1050–1065.

Tomita, H., M. Tsugawa, M. Satoh, and K. Goto, 2001: Shallow water model on a modified icosahedral geodesic grid by using spring dynamics. *J. Comput. Phys.*, **174**, 579–613.

Wiin-Nielsen, A., 1959: On the application of trajectory methods in numerical forecasting. *Tellus*, **11**, 180–196.

Williamson, D. L., and P. J. Rasch, 1989: Two-dimensional semi-Lagrangian transport with shape-preserving interpolation. *Mon. Wea. Rev.*, **117**, 102–129.

Williamson, D. L., J. B. Drake, J. J. Hack, R. Jackob, and P. N. Swarztrauber, 1992: A standard test for numerical approximations to the shallow water equations in spherical geometry. *J. Comput. Phys.*, **102**, 211–224.

Xiao, F., T. Yabe, X. Peng, and H. Kobayashi, 2002: Conservative and oscillation-less atmospheric transport schemes based on rational functions. *J. Geophys. Res.*, **107**(D22), 4609, doi: 10. 1029/2001JD001532.